RSC Advances

ROYAL SOCIETY OF CHEMISTRY

www.rsc.org/advances

RSC Advances

RSCPublishing

ARTICLE

Direct Manipulation of Particle Size and Morphology of Ordered Mesoporous Silica by Flow Synthesis†

Cite this: DOI: 10.1039/xoxxoooooox

T. N. Ng,[a,b] X.Q. Chen,[a,c] and K. L. Yeung*[a,d]

Received ooth January 2012,
Accepted ooth January 2012

DOI: 10.1039/xoxxoooooox

www.rsc.org/

The precision by which the fluid mixing, flow pattern, and reaction can be manipulated in a *flow-synthesis* reactor enables the deliberate preparation of ordered mesoporous silicas (OMS) of controlled particle size (ca. 50 to 650 nm) and shapes (i.e., spheres and random), as well as complex microstructures (i.e., hollow spheres). Fluid mixing and flow pattern were generated using Tee- and slit interdigital micromixers under laminar and Taylor flow conditions, while hydrolysis reactions was governed by the alkoxide precursors (i.e. TEOS & TMOS) and temperature. The hollow OMS spheres can host molecules and clusters as demonstrated by the incorporation of ferrocene and iron nanoparticles.

1 Introduction

Microfluidic reactor offers a number of advantages for solid preparations.[1–7] Yonemoto's work[1] is among the first to pioneer the flow synthesis of solids. Their work showed that TiO_2 particles prepared under Taylor flow (i.e., slug flow) were more uniform in size than TiO_2 produced under laminar flow conditions. This was followed by the work of Khan *et al.*[2] on the synthesis of colloidal SiO_2 in a microfluidic reactor. The synthesis was carried out under Taylor flow in square microchannels (i.e., 50 μm wide and 150 μm deep), where the micromixing within the liquid slugs produces mono-dispersed SiO_2 sol. Precise control of particle size was obtained by simply changing the reaction time. Numerous metal nanoparticles have been successfully prepared in microreactors.[3,4] Uniform silver nanoparticles were obtained from a setup consisting simply of a syringe pump, tubular coil and heating bath.[3] Although the reaction was carried out under laminar flow, the rapid heat transfer allows precise temperature control enabling direct control on the nucleation and growth of the nanoparticles.

Quantum dots, porous solids and nano-assemblies are examples of complex solids prepared in microreactors.[5] Kikkeri *et al.*[7] employed three microfluidic chips kept at different temperatures to produce carbohydrate-functionalized CdSe/ZnS and CdTe/ZnS quantum dots of narrow size distributions. Numerous metal-organic frameworks (MOFs) crystals were successfully produced in microreactors.[9] Faustini *et al.*[10] prepared magnetic MOF by embedding magnetic nanoparticles during their synthesis. Several recent works discussed the synthesis of complex assemblages using microreactors.[9,11] Phase mixing and droplet breakdown can be precisely controlled by manipulating the flow streams allowing the preparation of Janus particles. The precise assembly of core-shell particles has also been demonstrated in microreactors.[12,13] Nie and coworkers[12] were able to manipulate in their work the number and location of core particles within poly(tripropylene glycol diacrylate) shell.

This work investigates the flow-synthesis of ordered mesoporous silica (OMS), which has applications in chemical reaction and separation[14–17], electronics and sensors[18-20], and for drug-delivery and biomedicine[21–23]. Supra-molecular templating method is commonly used to prepare OMS, and involves the self-assembly of the template molecules, the hydrolysis of silica precursor and their reaction and condensation on the template to form embryonic seeds, followed by nucleation and growth.[24–27] The precision by which flow, mixing and temperatures could be controlled within the microreactor makes it an ideal tool to investigate their effects on the formation of complex solids such as OMS.

[a]*Department of Chemical and Biomolecular Engineering, The Hong Kong University of Science and Technology, Clear Water Bay, Kowloon, Hong Kong S.A.R., PR. China.*

[b]*Energy Technology Concentration Program, The Hong Kong University of Science and Technology, Clear Water Bay, Kowloon, Hong Kong S.A.R., PR. China.*

[c] *Shanghai Advanced Research Institue, Chinese Academy of Science, Shanghai, China.*

[d]*Division of Environment, The Hong Kong University of Science and Technology, Clear Water Bay, Kowloon, Hong Kong S.A.R., PR. China.*

† Electronic Supplementary Information (ESI) available: The length of slugs in stable Taylor flow as a function of U_{Gs}/U_{Ls}, CFD calculations of velocity and concentration profiles in micromixers under balanced and unbalanced flow conditions, morphology and size of OMS particles prepared from TMASi, and XRD of OMS particles prepared by batch synthesis with addition of DMHA at 0oC. See DOI: 10.1039/b000000x/

2 Experimental methods

Materials. Tetraethylorthosilicate (TEOS, 98 %), tetramethylorthosilicate (TMOS, 98 %), tetramethylammonium silicate solution (TMASi, 15-20 wt. % in H_2O), cetyltrimethylammonium bromide (CTABr, 99.3 %), N, N-dimethylhexadecylamine (DMHA, ≥ 95 %) and Di(cyclopentadienyl)-iron (Ferrocene, 98 %) were purchased from Sigma-Aldrich and used without further preparation. Sodium hydroxide (≥ 98 %, VWR), ammonium hydroxide (Fisher Scientific), hydrochloric acid (37 %, Acros), ammonium chloride (99.6 %, Acros) and absolute ethanol (Panreac) were used as received.

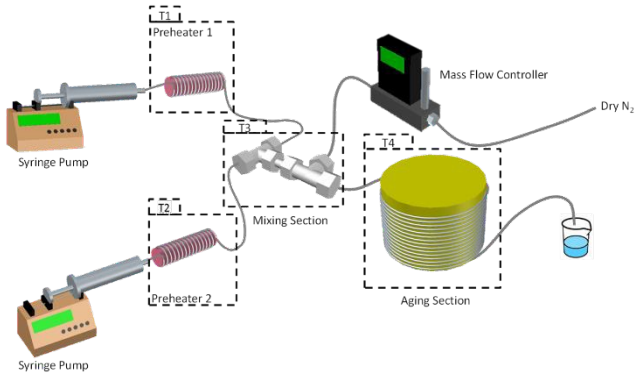

Figure 1 A schematic diagram of the flow synthesis reaction setup for laminar and Taylor flow operations.

Synthesis. An aqueous CTABr solution (Solution A) of desired concentration was obtained by dissolving a measured amount of CTABr powder in alkaline NaOH or NH_4OH solution. A silicon alkoxide solution (solution B) was prepared by adding the correct amounts of TEOS or TMOS in absolute alcohol to give the desired Si/CTA^+ mole ratio in the final reaction mixture. DMHA can also be added as a co-solute to adjust the pore size and morphology of the mesoporous silica. In an experiment, ferrocene was dissolved in DMHA and introduced as precursor for iron particles. Solutions A and B were filtered to remove solids and 20 ml of the respective solutions were drawn into separate 25 ml syringes, careful that air bubbles are not entrained. The syringes were then placed in two syringe pumps (KD Scientific KDS 100) that can deliver flow rates of 0.1 to 200 $ml.h^{-1}$ up to a pressure of about 3 bar. The pH of the reaction mixture was measured by a Thermo Orion pH meter. Figure 1 shows that in the reaction setup, solutions A and B were respectively preheated to T1 and T2, before entering the micromixing and aging sections that were kept at temperatures T3 and T4, respectively. The separate heating stages allow a precise control of the temperature during mixing, reaction and growth of the ordered mesoporous silica. A Tee micromixer (T-mixer) and a slit interdigital micromixer (SIM) were used in the study. The SIM was purchased from IMM (Mainz, Germany) and has a stainless steel inlay containing 16 inter-digitated channels (45 μm x 200 μm) on each side that guide the mixing of the two fluid streams. The mixed fluid exits through a narrow 40 μm x 4500 μm slit. The flow leaving the micromixing section enters the 8 m ageing section made of Teflon capillary tube with an inner diameter of 1.58 mm. The flow was varied from laminar to Taylor flow by adjusting the liquid and gas superficial velocities (i.e., U_{GS} = 0 for laminar flow). The product mixture was quenched by dilution in cold, deionized distilled water and recovered by a series of centrifugation steps. The recovered solids were dried and then calcined at 823 K for 12 h.

Table 1 summarizes the synthesis compositions and reaction conditions investigated in this study. The effects of mixing (*1*) on the quality of the mesoporous silica were examined for Tee- and slit interdigital micromixers for balanced and unbalanced flows. Different silicon alkoxide precursors have different hydrolysis rates and produce different hydrolyzed species. The hydrolysis rate (*2*) could be manipulated by using combinations of alkoxide precursors in different proportions. Table 1 lists the compositions of TEOS and TMOS used for the flow-synthesis of mesoporous silica under Taylor flow conditions. Co-solutes are often added to manipulate the pore size of mesoporous silica, and the addition of DMHA was performed for the synthesis of mesoporous silica in both Tee- and slit interdigital micromixers under laminar and Taylor flow conditions (*3*).

Table 1 Flow synthesis of OMS particles

Solutions		Fluid Flow (ml/min)			Flow Type	T (°C)				Micromixer Type	Residence Time (min)
A	B	A	B	N_2		1	2	3	4		
(1) Balanced and unbalanced flows											
1 CTAB:292 NH_4OH:1460 H_2O	6.6 TEOS:775 EtOH	0.3	0.3	0	Laminar (balanced)	25	25	25	65	SIM	9
1 CTAB:5070 H_2O	8.1 TMASi:1770 EtOH	0.6	0.6	1.8	Taylor (balanced)	25	25	25	25	SIM/T-mixer	5
1 CTAB:2.6 NaOH: 10100 H_2O	8.7 TEOS:51 EtOH	1.2	0.03	1.8	Taylor (unbalanced)	75	25	75	85	T-mixer	5
(2) Particle size											
1 CTAB:2.6 NaOH:10100 H_2O	8.7 TEOS:51 EtOH 8.3 TEOS:0.4 TMOS:51 EtOH 8.1 TEOS:0.7 TMOS:51 EtOH 7.9 TEOS:0.9 TMOS:51 EtOH 7.6 TEOS:1.1 TMOS:52 EtOH 7.4 TEOS:1.3 TMOS:52 EtOH	1.2	0.03	1.8	Taylor (unbalanced)	75	25	75	85	T-mixer	5
(3) Particle morphology											
1 CTAB:292 NH_4OH:1460 H_2O	6.6 TEOS:2 DMHA: 775EtOH	0.3	0.3	0	Laminar (balanced)	0 25 45	0 25 45	0 25 45	65 65 65	SIM	9
1 CTAB:292 NH_4OH:1460 H_2O	6.6 TEOS:2 DMHA: 775EtOH	0.1	0.1	0.4	Taylor (balanced)	0	0	0	65	T-mixer	9

Characterization. The products of the flow-synthesis in the microreactor were imaged by scanning electron microscope (JEOL JSM-6300F) and transmission electron microscope (JEOL JEM 2010) to determine the particle size and morphology as well as the pore structure. The dried sample was dispersed in ethanol under ultrasonic vibration. Samples for SEM imaging were deposited on silicon wafer, coated with a thin layer of gold and mounted on the sample holder. The SEM images were analysed by ImagePro software to determine the particle size and size distribution. Samples for TEM were deposited on holey carbon film Cu TEM grid and imaged at an accelerating voltage of 200 kV and a beam current of 100 pA/cm^2. X-ray diffraction of the products were carried out in the PANalytical X'pert Pro X-ray diffractometer equipped with a Cu Kα X-ray source (λ =1.5418 Å), at 45 kV and 40 mA. The diffraction data were collected between 2θ = 2 to 10˚ with 0.033˚ step size and a 30 s counting time using a standard slit configuration. Nitrogen physisorption measurements were done in the Coulter SA 3100 after the sample had been outgassed in vacuum at 403 K for 2 h. The specific surface area of the samples was calculated by Brunauer-Emmett-Teller (BET) method and the pore volume was determined from the adsorbed N_2 at P/P_0 = 0.984. The pore size distribution was calculated by both Barrett-Joyner-Halenda (BJH) and Kruk methods.[13,25,28,29]

3 Results and Discussion

The flow synthesis of solids in microfluidic system is complex, and can involve reactions, nucleation, crystallization, growth and aggregation.[2,4,10,12] Each being sensitive to temperature, pH and composition of the fluid. Furthermore, solid formation alters the fluid properties (e.g., density and viscosity) and flow characteristics (i.e., slurry flow).[30–33] Indeed, Einstein shows that fluid viscosity changes with the concentration of suspended spherical particles according to:

$$\eta_{bulk} = \eta_{liquid}(1 + 2.5C) \quad (1)$$

where C is the volumetric concentration of the slurry. This equation was further refined by Thomas[34] for particles between 100 nm to 400 μm:

$$\eta_{bulk} = \eta_{liquid}(1 + 2.5C + 10.05C^2 + 0.00273e^{16.6C}) \quad (2)$$

Solids can induce non-Newtonian flow with particle-to-particle and particle-to-wall interactions being non-negligible[32,35,36]. The situation is further complicated by the use CTA^+, a surfactant molecules, as SDA for the synthesis of OMS particles. Surfactants can alter the dynamics of the solids' interactions with the suspending fluid, other solids and the channel walls. This makes *a priori* prediction of the synthesis conditions difficult if not impossible.

Experiments were performed to identify a stable operating window for the flow synthesis of OMS particles. These are listed in Table 2. The temperature was kept significantly below the bubble point of the suspension (i.e., T ≤ 85°C), while the pressure was adjusted to suppress evaporation (i.e., P = 1.2 bar). The liquid flow (i.e., 0.2 to 1.5 ml/min) was adjusted to give sufficient time for reaction, assembly, nucleation and growth of OMS particles, but kept fast enough to inhibit excessive wall deposition that could lead to flow blockage. The gas flow was adjusted to generate Taylor flow with long fluid segments (i.e., (i.e., L_S/d > 10) to avoid shear-induced micelle breakup that could affect OMS formation[37–39]. The gas flow was kept between 1.8 ± 0.1 sccm in order to maintain a stable segmented flow (Fig. S1 in SI).

Table 2. Operational window for flow synthesis of OMS particles

Temperature (ºC)	25~85
Pressure Drop in the slug (Pa)	less than $5x10^{-2}$
U_{GS}/U_{LS}	1~10
U_{GS} (m/s)	0.013~0.024
U_{LS} (m/s)	0.0024~0.013

3.1 Synthesis under Balanced and Unbalanced Flows

The synthesis of ordered mesoporous silica (OMS) was performed under balanced and unbalanced flow conditions. Micromixers are designed to have the best mixing when the two fluid streams are of similar flows[40–43]. Computational fluid dynamics calculations showed that fluid mixing is more efficient in the slit interdigital micromixer (SIM) compared to the Tee micromixer (Figs. S2a & S2b in SI). The mixing can be enhanced by generating Taylor or segmented flow, where the shear between the wall and moving fluids produces internal circulation within the fluid slugs. OMS particles were prepared from 6.6 TEOS: 1 CTA^+: 775 EtOH: 292 NH_4OH: 1460 H_2O under balanced flow conditions using a slit interdigital micromixer (SIM) with a laminar flow and a Tee micromixer with a Taylor flow. Figures 2a and 2b are scanning electron micrographs of the OMS particles obtained from the SIM and T-mixer, respectively. Comparable particle morphology was obtained from the two micromixers.

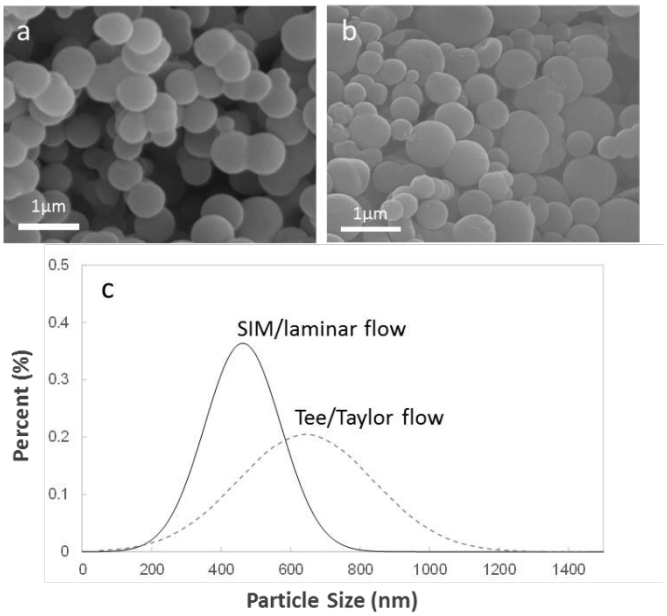

Figure 2 SEM images of OMS particles prepared by flow synthesis using a) SIM under laminar flow and b) T-mixer under Taylor flow, and c) their corresponding particle size distributions.

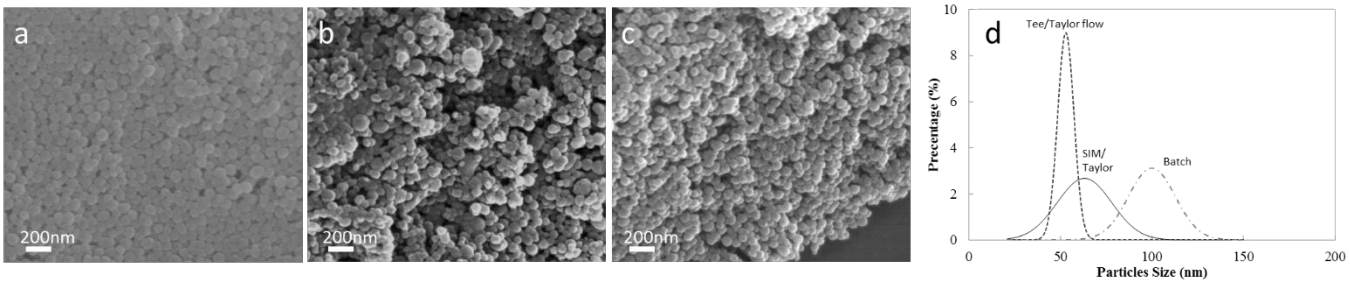

Figure 3 SEM images of OMS particles prepared from a) batch synthesis, and flow synthesis under unbalanced flow using b) SIM and c) T-mixer, and d) their corresponding particle size distributions.

Figure 2c shows that a narrower particle size distribution (PSD) is obtained from SIM (i.e., 460 ± 110 nm) compared to the Tee micromixer (i.e., 640 ± 190 nm) with corresponding coefficient of variance (COV) of 0.24 and 0.30. The rapid mixing of the reactant streams in SIM resulted in near instantaneous supersaturation and uniform nucleation producing OMS particles of narrow PSD as shown in the figure. The mixing in the T-mixer on the other hand, is limited by the diffusion of the reactants[42], and supersaturation is confined along the fluid interface where nucleation occurs. Further mixing occurred within the individual liquid slugs generated by the Taylor flow. The sustained liquid circulation within the slugs means fast mass transfer rates that also benefit crystal growth. This could explain the larger particles obtained from the Tee microreactor as shown in Fig. 2c.

The internal circulation within the fluid slugs in the Taylor flow is governed by the Bond number ($Bo = \frac{\Delta\rho g L^2}{\sigma}$ where $\Delta\rho$ is the difference in the density of the two fluids, g is the gravitational force, L is the characteristic length of the channel, and σ is the surface tension) that measures the relative contribution of surface tension and gravitational forces, and the capillary number ($Ca = \frac{\mu_l U_b}{\sigma}$) where μ_l is the liquid viscosity, U_b is the bubble velocity) that compares the effects of viscous forces and surface tension acting on the fluid interface[39].

The effects of gravity on the bubble velocity (U_b) can be neglected for narrow channels when $Bo < 1$,[39] thus allowing the liquid film thickness (δ) on the channel to be calculated from the capillary number[39]. Taylor *et al.*[44] correlated the Ca (between 5×10^{-5} to 3×10^{-1}) to the dimensionless film thickness (δ/r, where r is the channel diameter). Chen *et al.*[46] demonstrated that by monitoring the movement of an indicator bubble it is possible to calculated the liquid film thickness accurately from:

$$\frac{\delta}{r} = 0.5Ca^{\frac{1}{2}} \quad (3)$$

The relative thickness of the liquid film in our flow synthesis setup was 1.0×10^{-2} or 7.9 μm. This is sufficiently thin that liquid bypass can be neglected. Bretherton *et al.*[45] estimated the relative velocity of gas and liquid (m) from Ca.

$$m = 1.29(3Ca)^{\frac{2}{3}} \quad (4)$$

A calculated m value of 0.015 was obtained for the flow synthesis, which is much smaller than the critical value of 0.5 below which internal circulation dominates bypass flux[39,44].
The intensity of internal circulation is characterized by the recirculation time (T_L) that measures the time for a particle to move from one end of the liquid slug to the opposite end. The ratio of T_L to the residence time (τ) gives the dimensionless τ':

$$\tau' = \frac{T_L}{\tau} \quad (5)$$

In a channel with a circular cross-section, τ can be calculated from U_b and the overall superficial velocity (J) according to equation (6).

$$T_L = \tau\gamma\left(\frac{J}{U_B} - \frac{1}{2}\right)^{-1} \quad (6)$$

where γ is the relative length of the liquid slug to that of the capillary. The recirculation time (T_L) and the dimensionless τ' for the experiment were 2.2 s and 1.5×10^{-2}, respectively. The τ'/γ value of 6.9 is comparable to that reported in literature for Taylor flow including that of Kashid *et al.*[46] (τ'/γ =2.5), Thulasidas *et al.*[47] (τ'/γ =2.0) and Zaloha *et al.*[48] (τ'/γ =2.5) with a two-fold increase in mixing intensity compared to a laminar flow[38].

It is not uncommon in material synthesis due to the reaction stoichiometry for the quantity of the reactants, and thus the size of the mixing streams to differ significantly. The synthesis of OMS particles from 8.7 TEOS: 1 CTA^+: 51 EtOH: 2.6 NaOH: 10,100 H_2O requires an unbalanced flow. It is not possible to prepare OMS particles from SIM with laminar flow under this situation, as solid depositions in the micromixer and on the tube wall near the SIM outlet caused complete flow blockage within few minutes of operation. Computational fluid dynamics (CFD) calculations identified stagnant regions in both SIM's interdigital inlay and the outlet slit (Fig. S3a in SI) that could lead to solid depositions. The high pressure generated at the slit entrance dislodged some of the deposited solids and the flow carries the solids downstream to deposit on the tube wall. The resulting deposit built-up destabilized and eventually stopped the flow. Taylor flow can ameliorate the situation by preventing solid deposition on the ageing section for a sufficient time (ca. 1 h) to collect enough samples for analysis.

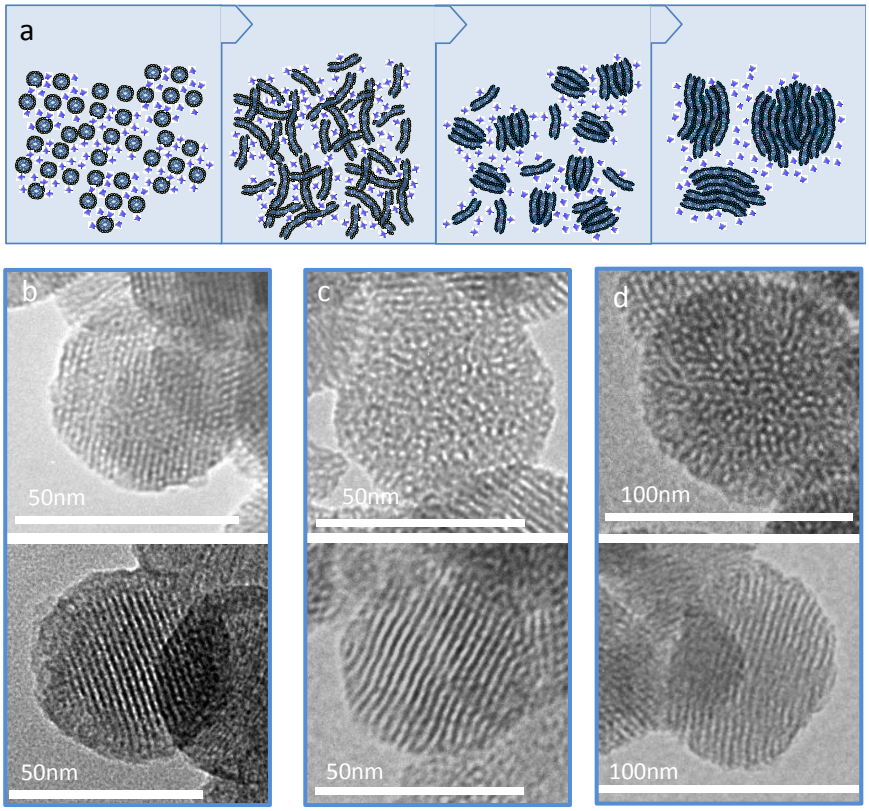

Figure 4 a) A schematic drawing of the genesis of OMS particles and their respective transmission electron micrographs as obtained from the flow synthesis of 8.7 SiO_2: 1 CTABr: 2.6 NaOH: 51 EtOH: 10,100 H2O with b) TEOS, c) 12.3 TEOS: 1 TMOS and d) 5.7 TEOS: 1 TMOS for SiO_2 source.

Figures 3a & 3b compares the OMS particles obtained from a batch synthesis and the flow synthesis using SIM with Taylor flow. Particles from flow synthesis appear to have a more irregular shape that could be a result of flow perturbations caused by surface depositions in SIM and ageing tube. The PSD plots in Fig. 3d shows that smaller particles were obtained from the flow synthesis. The distribution width is comparable to particles obtained from the batch synthesis suggesting a relatively similar degree of mixing.

A computational modeling study done by Roudgar and coworkers[49] showed that in laminar flow (Re = 1), mixing in a Tee micromixer is better under unbalanced flow conditions than under balanced flow. They argued that the shift of fluid interface towards the wall slows the flow allowing a longer time for diffusion. The same situation was observed in our study, and as the flow differential is large (i.e., 1:40), the fluid interface is near the micromixer's wall as shown in Fig. S3b in SI. However, this can pose a problem in solid synthesis as it can promote wall depositions. This could be particularly serious for OMS synthesis due to the presence of CTA^+ surfactant molecules. Wall deposition was avoided by using Taylor flow to generate internal mixing in the fluid leaving the Tee micromixer. The *Bo* ranges between 0.34 to 0.38, and this gives a relative liquid film thickness of 9.2×10^{-3} (15 μm). A recirculation time (T_L) of 1.4 s and a dimensionless τ' of 5.1×10^{-3} were obtained indicating a good internal mixing. It can be seen from the electron micrograph in Fig. 3c that the OMS particles prepared from the Tee micromixer with Taylor flow are smaller and more uniform in size and shape. The PSD shows a coefficient of variation (COV) of 0.08 as compared to 0.22 and 0.16 for SIM with Taylor flow and batch syntheses, respectively.

3.2 OMS Particle Size

It has been postulated that silica species in the synthesis mixture assist in the self-assembly of the organic structure directing agents (SDA) during the formation of OMS[50] as shown in the schematic drawing in Fig. 4a. The CTA^+ SDA catalyzes the hydrolysis of the organic silica and stabilizes the oligomeric silicate anion. Solid particles with rigid walls are eventually formed by the condensation and polymerization of the silica.[51] Different silicon alkoxide precursors have different hydrolysis rates and generate different hydrolyzed species.[52] The relative hydrolysis rate of TMOS to TEOS is estimated to be 8 from the rate coefficient of hydrolysis of Si-OR group to Si-OH in basic medium (i.e., 2.35 x $10^{-3}M^{-1}s^{-1}$ for TMOS and 0.29 x $10^{-3}M^{-1}s^{-1}$ for TEOS).[53]

Figures 4b-d are transmission electron micrographs of OMS particles obtained from 8.7 SiO_2: 1 CTABr: 2.6 NaOH: 86-*x* EtOH: *x* MEOH: 10,100 H_2O synthesis mixture, but with SiO_2 from TEOS (Fig. 4b), 12.3 TEOS: 1 TMOS (Fig. 4c) and 5.7 TEOS: 1 TMOS (Fig. 4d). The reactant feeds were mixed with a T-mixer under unbalanced flow condition and a segmented

Table 3 Properties of OMS particles

Solution A	Solution B	Flow Type	Mixing Temperature (°C)	Particle dimension (nm) Diameter (D_0)	Cavity (D_1)	D_0-D_1	S_{BET} ($m^2 \cdot g^{-1}$)	d_{100}(Å)	Pore(Å) BJH w_{BJH}	BJH t_{BJH}	Kruk w_{Kruk}	Kruk t_{Kruk}
Size Control												
1CTAB/2.55NaOH/10100H_2O	8.7TEOS /51EtOH	Batch	85	80±13	--	--	1091	38	29	15	34	10
	8.7TEOS /51EtOH	Tee/Taylor (unbalanced)	75	53±4	--	--	982	40	26	20	33	13
	8.1TEOS/0.7TMOS/51 EtOH			62±11	--	--	903	36	22	19	28	13
	7.4TEOS/1.3TMOS/52.00 EtOH			82 ±14	--	--	848	36	23	18	28	14
Morphology control (hollow vs solid)												
1CTAB/292NH_4OH/1460H_2O	6.6TEOS/2DMHA/775EtOH	SIM/Laminar (balanced)	0	690±130	600±150	90±20	470	40	40	7	26	21
			25	630±170	470±210	160±40	1130	40	39	7	30	16
			45	630±150	--	--	300	36	37	4	34	8
		Tee/Taylor (balanced)	0	640±190	--	--	872	--	38	--	--	--
1CTAB/292NH_4OH/1460H_2O	6.6TEOS/2DMHA/775EtOH	Batch	0	--	--	--	841	42	29	21	31	18
			25	--	--	--	709	37	26	16	24	18
			45	--	--	--	992	40	29	17	31	15
1CTAB/292NH_4OH/1460H_2O	6.6TEOS/775EtOH	Batch	25	--	--	--	--	--	28	--	32	--

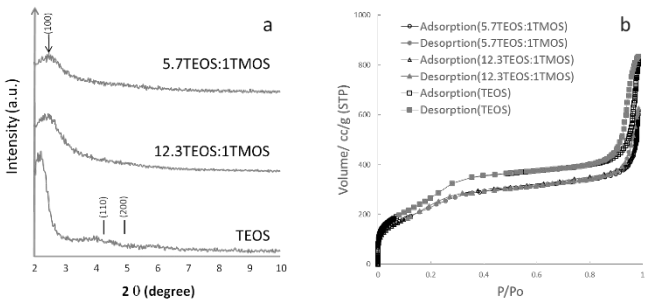

Figure 5 a) XRD and b) N_2 physisorption-desorption isotherms of OMS particles prepared by flow synthesis (T-mixer Taylor flow) of 8.7 SiO_2: 1 CTABr: 2.6 NaOH: 51 EtOH: 10,100 H2O with TEOS, 12.3 TEOS: 1 TMOS and 5.7 TEOS: 1 TMOS for SiO_2 source.

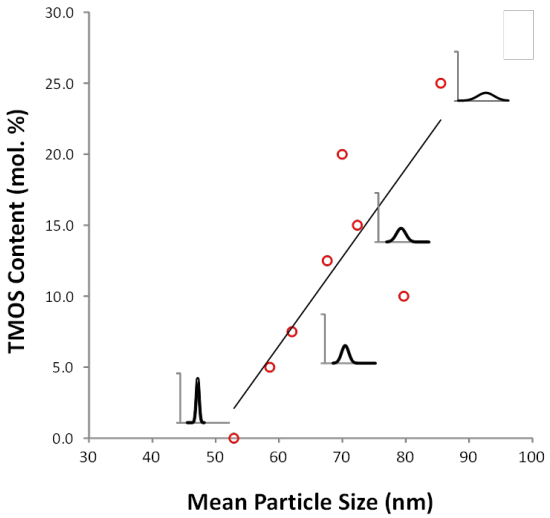

Figure 6. Plots of the mean particle size and particle size distribution (inset) of the OMS prepared by flow synthesis for different TMOS content.

Taylor flow was obtained by adjusting the liquid and N_2 gas flows to 1.5 ml.min^{-1} and 1 sccm, respectively. According to the work of Triplette *et al.*[54], these flow conditions fall within the slug flow regime with stable gas and liquid flows along the channel. A reaction residence time of 5 min was maintained for all the synthesis, and each synthesis run lasts for 1 h producing about 0.05 g of recoverable solids that is equivalent to a yield of about 15 percent. The samples were taken directly from the quenched solutions and observed under TEM.

The particles prepared from TEOS as silica source have well-ordered hexagonal pore structures and straight pore channels as shown by Fig. 4b. The particles are also more uniform in size with an average diameter of 53 ± 4 nm (i.e., COV = 0.08). The addition of TMOS resulted in a faster hydrolysis that also generated oligomeric silicate anion species. The pores of the produced particles display greater disorder as seen in the micrographs of Figs. 4c & 4d. The pore channels also appear to be irregular with the width varying along the length. This is consistent with the results of the X-ray diffraction in Fig. 5a, where the disappearance of the (110) and (200) diffraction peaks and broadening of the (100) peak indicate growing disorder in the pore structure with the addition of TMOS. The pore size distributions determined by Barrett-Joyner-Halenda (BJH) method from the N_2 physisorption experiments (Fig. 5b) are summarized in Table 3. The pore diameter and wall thickness were also calculated according to Kruk's equation and listed in the table. Samples prepared from pure TEOS from both batch and flow syntheses have a pore diameter of 3.3 nm and wall thickness of 1.0-1.3 nm similar to values found in MCM-41.[19,55,56] The pore diameters of particles prepared with TMOS are significantly narrower than 3.3 nm with thicker walls. The hysteresis at a relative high pressure (P/Po=0.9) originated from inter-particle porosity.[57]

Reactions occur upon mixing of the reactants in the T-mixer and continued within the well-mixed liquid slugs generated by the Taylor flow. Hydrolysis of silicon alkoxides generates different silicate species in the solution and alters the solution chemistry[53]. TMOS which hydrolyzes more readily than TEOS produces more hydrolyzed silicate species that reacts with the

CTA^+ SDA to generate the self-assembled silicate worm-like micelles as shown in Fig. 4a. The worm-like micelles aggregate and anneal into rod-like micellar structures that are precursor to the pore channels of the OMS particles. A rigid wall is formed with the condensation and polymerization of the silicates and this solidifies the structure forming a nucleus for growth of the OMS particles. Figure 6 shows that larger particles were obtained as the proportion of TMOS in the silicon alkoxide mixture is increased. Synthesis from pure TEOS gave particles of 53 ± 4 nm, while larger particles of 62 ± 11 nm and 82 ± 14 nm were obtained when 7.5 and 15 mole % TMOS were used. Indeed, the plot shows a linear relation between particle size and TMOS content in the synthesis mixture. Besides having larger particle size, the particle size distribution is also wider in samples prepared from higher TMOS content with COV of 0.08, 0.17 and 0.21 for 0, 7.5 and 15 mole % TMOS, respectively. The particles are also more irregular in shape. In the extreme case of using a fully hydrolyzed silica source (i.e., TMASi), irregular particles were formed. These particles are aggregates of smaller OMS particles of roughly 170±80 nm in diameter as shown in Fig. S4 in SI. It is also clear from the TEM picture (cf. Fig. S4b in SI) that the pore channels are more worm-like and less uniform in width. In this situation, the silica wall had formed rapidly, solidifying and freezing the shape and structure of the pores and particles.

3.3 Hollow OMS Particles

Co-solutes such as trimethylbenzene and DMHA are often added to stabilize the formation of worm-like micelles and to manipulate the pores of the mesoporous silica.[58–61] DMHA is a natural thermal decomposition byproduct of CTA^+ SDA and is highly compatible with the SDA.[13,60] It has been used as pore expander by various authors[58] to obtain mesopores as large as 13.5 nm, but DMHA can interfere with the assembly of silica-SDA mesophase resulting in poorer structural order.[60] Indeed, batch syntheses prepared from 6.6 SiO_2: 1 CTABr: 2 DMHA: 290 NH_4OH: 775 EtOH: 1460 H_2O at 45, 25 and 0°C produce solid OMS particles (cf. Figs. 7a-7c). OMS with progressively larger pores of 2.6, 3.0 and 3.4 nm were obtained with increasing synthesis temperatures as listed in Table 3. The products also display greater structural disorder particularly for samples prepared at lower temperatures (Figs. S5 in SI).

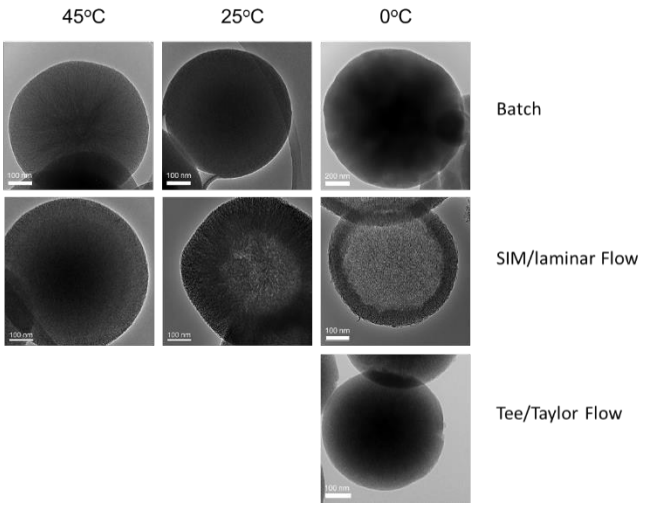

Figure 7 TEM images of the sample prepared in batch (a-c) and flow syntheses (d-g) at feed and mixing temperatures of a) & d) 45°C, b) & e) 25°C and c), f) & g) 0°C.

The flow synthesis of OMS with DMHA co-solutes was carried out in SIM under laminar flow. The feed and mixing temperatures were varied from 45, 25 to 0°C, while keeping the ageing temperature constant at 65°C. Similar to batch synthesis, solid OMS particles were obtained at 45°C as shown in Fig. 7d. Lowering the temperature to 25°C yield hollow OMS particles with a shell thickness of 160 ± 40 nm as shown in Fig. 7e. Hollow OMS particles with a thinner shell of 90 ± 20 nm, were obtained at 0°C (cf. Fig. 7f). All OMS particles from the flow synthesis have a similar diameter of ca. 650 nm that is comparable to the particles obtained from the batch syntheses (Table 3). The hydrolysis of silicon alkoxides and to a lesser extent the micellation process depend on the temperature. The hydrolysis of TEOS is often approximated by a first order reaction rate equation.[62,63] Chen and coworkers[63] used Marquardt regression method to obtain the empirical hydrolysis rate constant K_h:

$$K_h = 74.36e^{(\frac{-E_a}{RT})}[H_2O]^{1.267}[NH_3]^{0.971} \quad (8)$$

where E_a = 25.2 kJ/mol, and with water and ammonia in excess, $[H_2O]$ and $[NH_3]$ are constant. Thus, the hydrolysis rate halves with each 20°C decrease in the temperature.

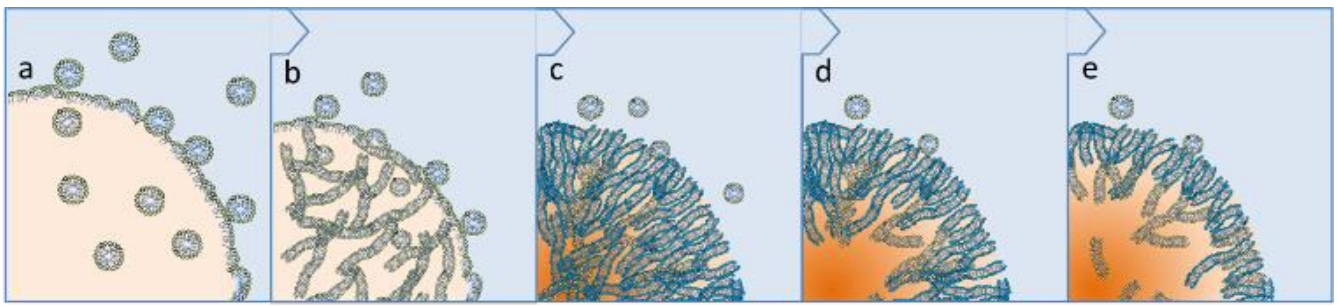

Figure 8 Proposed formation mechanisms for hollow OMS particles during mixing (a-c) and reaction (c-e) stages, where: a) generation of a stable emulsion droplet, and b) & c) formation of silicate-stabilized worm-like micelles within the emulsion droplet, d) & e) phase separation and formation of hollow shell structure.

In the flow synthesis, TEOS was dissolved in DMHA and ethanol, and will partition preferentially in DMHA within the core of the emulsion droplet as shown in Fig. 8a. The hydrolysis of TEOS is rapid at 45°C and occurs immediately on mixing producing hydrolyzed silicate species that interacts with CTA^+ to form stable silicate-SDA mesophase structures that eventually anneal into the final OMS structure as it travels along the ageing section (cf. Figs. 8a-8c). The structure solidifies with the condensation of the silicates. Lowering the temperature slows the hydrolysis of TEOS and the initial mesophase structure appears unstable and phase separation occurs within the worm-like micelle stabilized emulsions as illustrated in Figs. 8c-8d. In the ageing section kept at higher temperature, the hydrolysis of TEOS occurs at the interface with the alkaline water solution forming a thin skin of mesophase structure (Figs. 8d-8e). The growth of the skin is governed by the diffusion of the reacting species across the mesophase layer resulting in the hollow OMS particles shown in Figs. 7e and 7f. Lowering the temperature also has the effect of decreasing the yield with the relative mass of OMS estimated at 1.0, 0.6 and 0.4 for 45, 25 and 0°C samples, respectively.

It is postulated that micromixing suppresses phase separation in the batch synthesis so that only solid OMS were produced. A control experiment was performed in a T-mixer with Taylor flow to generate micromixing. Feed and mixing temperatures were kept at 0°C with the ageing section heated to 65°C as was the case in SIM with laminar flow. Figure 7g shows that solid OMS of comparable particle and pore sizes to the samples from the batch synthesis were obtained instead of hollow OMS. This confirms the importance of fluid mixing in solid synthesis and demonstrates the precision by which microfluidic system manipulates fluid flow and controls the flow synthesis of materials.

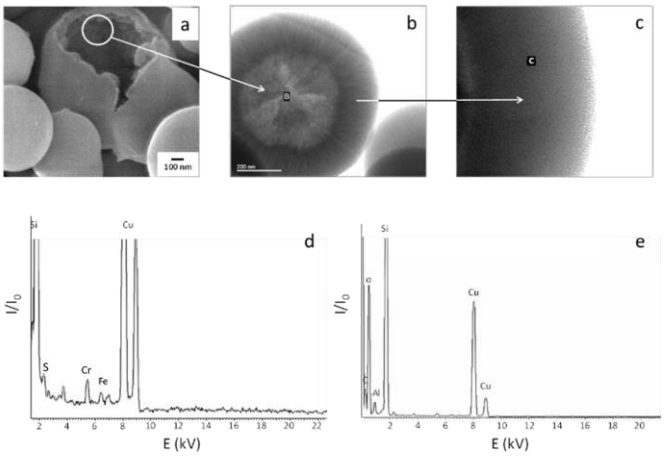

Figure 9 a) SEM and b) & c) TEM images of hollow OMS particles encapsulating iron nanoparticles prepared by a single-stage flow synthesis from ferrocene precursor. EDXS analysis of the core *(b)* and shell *(c)* indicate that d) iron is present on the core and e) the wall are free of iron that might hinder diffusion.

The observed phase separation phenomenon in Fig. 8 provides an interesting route for molecular and nanoscale storage. Ferrocene was introduced and stored in the core of the hollow OMS by simply dissolving the hydrophobic ferrocene in the TEOS/DMHA/EtOH solution and carry out the flow synthesis at low temperature (i.e., T1, T2, T3 = 0°C). Heat treatment in air at 500°C for 2 h converts the stored ferrocene into iron nanoparticles as shown in the SEM micrographs in Fig. 9. Iron nanoparticles uniformly decorated the inner surface of the 80 nm thick mesoporous silica shell (Fig. 9a). The iron nanoparticles measure less than 10 nm in diameter (Fig. 9b) and are confined mainly in the core of the hollow OMS spheres as confirmed by EDXS (Fig. 9d). Iron is not present in the mesopores of the shell according to both TEM examinations (Fig. 9c) and EDXS analysis (Fig. 9e). It was estimated that roughly 0.9 weight percent of ferrocene (ca. 80 %) was successfully stored and encapsulated within the hollow OMS.

Conclusions

This work clearly illustrated the opportunities of *flow synthesis* in the production complex porous solids. OMS was selected for the study not only because it is a versatile nanomaterial with a broad range of potential applications[64-66], but its preparation also encompasses two important nanomaterial synthesis routes, the templated synthesis and sol-gel processing. Besides the advantage of continuous flow production, solid synthesis is more rapid and energy efficient promising a cleaner production of nanoparticles. The precise manipulation of fluid mixing, flow pattern and reaction in *flow synthesis* allows unprecedented opportunity in *shaping* the OMS at nano- (i.e. pores), micro- (i.e. shape and morphology) and macroscales (i.e. aggregate, cf. Fig. S5 in SI) and provide new avenues for creating complex architectures and functionalities in these materials. It also serves as an analogue model for designing a microfluidic reactors,[67,68] particularly for solid synthesis.[69]

Acknowledgements

The authors gratefully acknowledge the financial funding from the Hong Kong Research Grant Council (HK GRF 606813). We thank Dr. K. F. Lam of the Division of Environment, HKUST for his advice and suggestions.

Notes and references

1 T. Yonemoto, M. Kubo, T. Doi and T. Tadaki, *Chem. Eng. Res. Des.*, 1997, **75**, 413–419.
2 S. A. Khan, A. Günther, M. A. Schmidt and K. F. Jensen, *Langmuir*, 2004, **20**, 8604–8611.
3 X. Z. Lin, A. D. Terepka and H. Yang, *Nano Lett.*, 2004, **4**, 2227–2232.
4 J. Wagner and J. M. Kohler, *Nano Lett.*, 2005, **5**, 685–691.
5 E. M. Chan, A. P. Alivisatos and R. A. Mathies, *J. Am. Chem. Soc.*, 2005, **127**, 13854–13861.
6 R. M. Sankaran, D. Holunga, R. C. Flagan and K. P. Giapis, *Nano Lett.*, 2005, **5**, 537–541.
7 R. Kikkeri, P. Laurino, A. Odedra and P. H. Seeberger, *Angew. Chem. Int. Ed.*, 2010, **49**, 2054–2057.
8 Z. Nie, W. Li, M. Seo, S. Xu and E. Kumacheva, *J. Am. Chem. Soc.*, 2006, **128**, 9408–9412.
9 N. J. Carroll, S. B. Rathod, E. Derbins, S. Mendez, D. A. Weitz and D. N. Petsev, *Langmuir*, 2008, **24**, 658–661.

10 M. Faustini, J. Kim, G.-Y. Jeong, J. Y. Kim, H. R. Moon, W.-S. Ahn and D.-P. Kim, *J. Am. Chem. Soc.*, 2013, **135**, 14619–14626.
11 L.-Y. Chu, A. S. Utada, R. K. Shah, J.-W. Kim and D. A. Weitz, *Angew. Chem. Int. Ed.*, 2007, **46**, 8970–8974.
12 I. Lee, Y. Yoo, Z. Cheng and H.-K. Jeong, *Adv. Funct. Mater.*, 2008, **18**, 4014–4021.
13 M. Kruk, M. Jaroniec and A. Sayari, *Langmuir*, 1997, **13**, 6267–6273.
14 T. Asefa, M. J. MacLachlan, N. Coombs and G. A. Ozin, *Nature*, 1999, **402**, 867–871.
15 T. Yokoi, H. Yoshitake and T. Tatsumi, *J. Mater. Chem.*, 2004, **14**, 951–957.
16 K. F. Lam, K. L. Yeung and G. McKay, *J. Phys. Chem. B*, 2006, **110**, 2187-2194.
17 K. F. Lam, C. M. Fong and K. L. Yeung, *Gold Bull.*, 2007, **40**, 192-198.
18 Y. Feng, R. Yao and L. Zhang, *Phys. B Condens. Matter*, 2004, **350**, 348–352.
19 I. I. Slowing, B. G. Trewyn, S. Giri and V. S.-Y. Lin, *Adv. Funct. Mater.*, 2007, **17**, 1225–1236.
20 B. J. Melde, B. J. Johnson and P. T. Charles, *Sensors*, 2008, **8**, 5202–5228.
21 M. Vallet-Regi, F. Balas and D. Arcos, *Angew. Chem.-Int. Ed.*, 2007, **46**, 7548–7558.
22 B. Munoz, A. Ramila, J. Perez-Pariente, I. Diaz and M. Vallet-Regi, *Chem. Mater.*, 2003, **15**, 500–503.
23 S. W. Song, K. Hidajat and S. Kawi, *Langmuir*, 2005, **21**, 9568–9575.
24 J. S. Beck, J. C. Vartuli, W. J. Roth, M. E. Leonowicz, C. T. Kresge, K. D. Schmitt, C. T. W. Chu, D. H. Olson and E. W. Sheppard, *J. Am. Chem. Soc.*, 1992, **114**, 10834–10843.
25 J. Y. Ying, C. P. Mehnert and M. S. Wong, *Angew. Chem.-Int. Ed.*, 1999, **38**, 56–77.
26 N. K. Raman, M. T. Anderson and C. J. Brinker, *Chem. Mater.*, 1996, **8**, 1682–1701.
27 Z. Zhang, J. Yin, H. J. Heeres and I. Melián-Cabrera, *Microporous Mesoporous Mater.*, 2013, **176**, 103–111.
28 D. D. Do, *Adsorption Analysis: Equilibria and Kinetics*, Imperial College Press, 1998.
29 A. Sayari, M. Kruk, M. Jaroniec and I. L. Moudrakovski, *Adv. Mater.*, 1998, **10**, 1376–1379.
30 K. Ekambara, R. S. Sanders, K. Nandakumar and J. H. Masliyah, *Ind. Eng. Chem. Res.*, 2009, **48**, 8159–8171.
31 E. J. Terrell and C. Fred Higgs, *J. Electrochem. Soc.*, 2006, **153**, K15.
32 S. Kuravi, University of Central Florida Orlando, Florida, 2009.
33 A. Kitanovski and A. Poredoš, *Int. J. Refrig.*, 2002, **25**, 827–835.
34 D. G. Thomas, *J. Colloid Sci.*, 1965, **20**, 267–277.
35 S. Sinha-Ray, S. Sinha-Ray, H. Sriram and A. L. Yarin, *Lab. Chip*, 2014, **14**, 494.
36 R. Sabbah, M. M. Farid and S. Al-Hallaj, *Appl. Therm. Eng.*, 2009, **29**, 445–454.
37 T. Abadie, C. Xuereb, D. Legendre and J. Aubin, *Chem. Eng. Res. Des.*, 2013, **91**, 2225–2234.
38 R. Gupta, D. F. Fletcher and B. S. Haynes, *Chem. Eng. Sci.*, 2010, **65**, 2094–2107.
39 P. Angeli and A. Gavriilidis, *Proc. Inst. Mech. Eng. Part C-J. Mech. Eng. Sci.*, 2008, **222**, 737–751.
40 V. Hessel, S. Hardt, H. Lowe and F. Schonfeld, *Aiche J.*, 2003, **49**, 566–577.
41 V. Hessel, H. Löwe and F. Schönfeld, *Chem. Eng. Sci.*, 2005, **60**, 2479–2501.
42 N. Nam-Trung and W. Zhigang, *J. Micromechanics Microengineering*, 2005, **15**, R1.
43 M. Hoffmann, M. Schlüter and N. Räbiger, in *Micro and Macro Mixing*, Springer, 2010, pp. 287–303.
44 G. I. Taylor, *J. Fluid Mech.*, 1961, **10**, 161–165.
45 F. P. Bretherton, *J. Fluid Mech.*, 1961, **10**, 166–188.
46 M. N. Kashid, I. Gerlach, S. Goetz, J. Franzke, J. F. Acker, F. Platte, D. W. Agar and S. Turek, *Ind. Eng. Chem. Res.*, 2005, **44**, 5003–5010.
47 T. C. Thulasidas, M. A. Abraham and R. L. Cerro, *Chem. Eng. Sci.*, 1997, **52**, 2947–2962.
48 P. Zaloha, J. Kristal, V. Jiricny, N. Völkel, C. Xuereb and J. Aubin, *Chem. Eng. Sci.*, 2012, **68**, 640–649.
49 M. Roudgar, E. Brunazzi, C. Galletti and R. Mauri, *Chem. Eng. Technol.*, 2012, **35**, 1291–1299.
50 C.-F. Cheng, Z. Luan and J. Klinowski, *Langmuir*, 1995, **11**, 2815–2819.
51 R. Xu, *Chemistry of zeolites and related porous materials: synthesis and structure*, John Wiley & Sons (Asia), Singapore; Hoboken, N.J., 2007.
52 T. N. M. Bernards, M. J. Van Bommel and A. H. Boonstra, *J. Non-Cryst. Solids*, 1991, **134**, 1–13.
53 B. Tan and S. E. Rankin, *J. Phys. Chem. B*, 2006, **110**, 22353–22364.
54 K. A. Triplett, S. M. Ghiaasiaan, S. I. Abdel-Khalik and D. L. Sadowski, *Int. J. Multiph. Flow*, 1999, **25**, 377–394.
55 J. Trébosc, J. W. Wiench, S. Huh, V. S.-Y. Lin and M. Pruski, *J. Am. Chem. Soc.*, 2005, **127**, 3057–3068.
56 Q. Cai, F. Z. Cui, X. H. Chen, Y. Zhang and Z. S. Luo, *Chem. Lett.*, 2000, 1044–1045.
57 V. Cauda, C. Argyo, A. Schlossbauer and T. Bein, *J. Mater. Chem.*, 2010, **20**, 4305–4311.
58 X. Zhou, A. Duan, Z. Zhao, Y. Gong, H. Wu, Y. Wei, G. Jiang and J. Liu, *Mater. Lett.*, 2014, **133**, 228–231.
59 M. Kruk, *Acc. Chem. Res.*, 2012, **45**, 1678–1687.
60 A. Sayari, Y. Yang, M. Kruk and M. Jaroniec, *J. Phys. Chem. B*, 1999, **103**, 3651–3658.
61 R. S. Franchi, P. J. E. Harlick and A. Sayari, *Ind. Eng. Chem. Res.*, 2005, **44**, 8007–8013.
62 M. T. Harris, R. R. Brunson and C. H. Byers, *J. Non-Cryst. Solids*, 1990, **121**, 397–403.
63 S.-L. Chen, P. Dong, G.-H. Yang and J.-J. Yang, *Ind. Eng. Chem. Res.*, 1996, **35**, 4487–4493.
64 K. F. Lam, C. M. Fong, K. L. Yeung and G. McKay, *Chem. Eng. J.*, 2008, **145**, 185-195.
65 X. Q. Chen, K. F. Lam, S. F. Mak and K. L. Yeung, *J. Hazardous Mater.*, 2011, **186**, 902-910.
66 X. Q. Chen, K. F. Lam and K. L. Yeung, *Chem. Eng. J.*, 2011, **172**, 728-734.
67 J. L. H. Chau, A. Y. L. Leung and K. L. Yeung, *Lab on a Chip*, 2003, **3**, 53-55.
68 W. N. Lau, K. L. Yeung and R. Martin-Aranda, *Microporous Mesoporous Mater.*, 2008, **115**, 156-163.
69 X. Q. Chen, T. N. Ng, M. Arruebo and K. L. Yeung, *Catal. Today*, 2013, **204**, 140-147.